CONEM 2016 CONGRESSO NACIONAL DE ENGENHARIA MECÂNICA
21 - 25 AGOSTO DE 2016 FORTALEZA - CEARÁ
ABCM 40 anos Associação Brasileira de Engenharia e Ciências Mecânicas

DYNAMICS OF SHAPE MEMORY ALLOY ORIGAMI-WHEEL

Larissa Maciel da Fonseca, larissamaciel.lah@gmail.com[1]
Guilherme Vieira Rodrigues, guilherme_@live.co.uk[1]
Marcelo Amorim Savi, savi@mecanica.ufrj.br[1]
Alberto Paiva, paiva.ufrj@gmail.com[2]

[1] Universidade Federal do Rio de Janeiro
COPPE – Department of Mechanical Engineering
Center for Nonlinear Mechanics
Rio de Janeiro – RJ – Brazil – 21.945.970 – P.O. Box 68.503

[2] Universidade Federal Fluminense
Volta Redonda School of Engineering
Department of Mechanical Engineering
Volta Redonda − RJ – Brazil – 27.255-250

Abstract: *Origami has inspired engineers to design compact systems with interesting abilities related to adaptive behavior. The use of smart materials increases the range of applicability of origami systems including robotics, biomedical and aerospace applications. Shape memory alloy (SMA) actuators are being used due to their capacity of generating high forces and deformations. This paper deals with the dynamical analysis of an origami-ball with SMA actuators. The origami-ball is usually employed in robotics presenting strong geometric and constitutive nonlinearities. Numerical simulations are carried out showing a complex dynamical response.*

Key-words: *origami, shape memory alloy, smart structures, nonlinear dynamics, chaos, robotics*

1. INTRODUCTION

The ancient Japanese art of paper folding, origami (oru (fold) and kami (paper)) creates a sculpture representation through pattern folds of a flat paper sheet producing a desired shape. Origami art starts to inspire researchers in order to produce systems and devices for various fields of science and technology (Peraza-Hernandez et al., 2014; Fei & Sujan, 2013). Basically, characteristics as self-adaptability and compacting capacities are motivating several applications. In essence, classical shapes as spheres, cylinders and also some combined forms of the folded shapes can be exploited assuming forms between two limit configurations, being useful for different purposes. This general idea can be employed on architectural design (Sorguç et al., 2009), robotics (Felton et al., 2014), aerospace systems (Nishiyama, 2012) and biomedical devices (Salerno, 2014).

The use of smart materials is an important issue for actuation of origami systems. Shape memory alloys (SMAs) and magnetic materials are of special interest due to their capacity to generate forces and displacements. Thus, it is possible to apply external fields (temperature, electric current or magnetic field) to induce the shape alteration of the origami between two desired configurations.

Since origami systems are slender structures, they are usually close to stability limits with important dynamical issues to be investigated. The combination of strong geometrical and constitutive nonlinearities is responsible for a rich dynamic behavior. Folding and operational excitations can affect the system response being critical to several applications. Therefore, dynamical response of origami systems is of special importance during design stage being the objective of this paper.

2. ORIGAMI-WHEEL PATTERN

This paper deals with the dynamic analysis of a robotic wheel. In essence, the origami wheel allows a structure to change from a cylindrical configuration to a flat circular shaped tube (Fig. 1). The waterbomb pattern (Fig. 2-b) is a well-known pattern that, repeated continuously, gives rise to the origami wheel pattern. Lee *et al.* (2013) redesigned the end of the origami wheel fold, giving rise to the wheel structure pattern (Fig. 2-a). Thus, is possible to transit between the two shapes (cylindrical tube and flat circular tube).

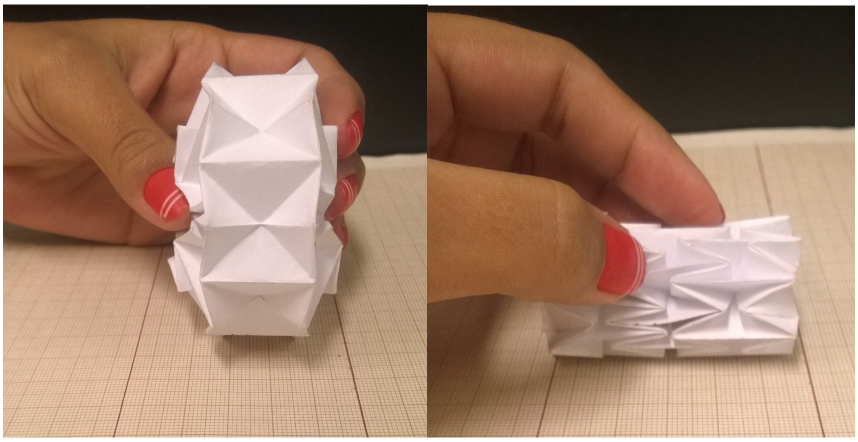

Figure 1 – Changing shape of the origami ball, going from a flat tube (left) to a circular tube (right).

The waterbomb and the origami wheel patterns were designed at Oripa. The unitary cell (Fig. 2-c) was designed using AutoCAD LT® software. Blue line means a valley fold and red line means a mountain fold.

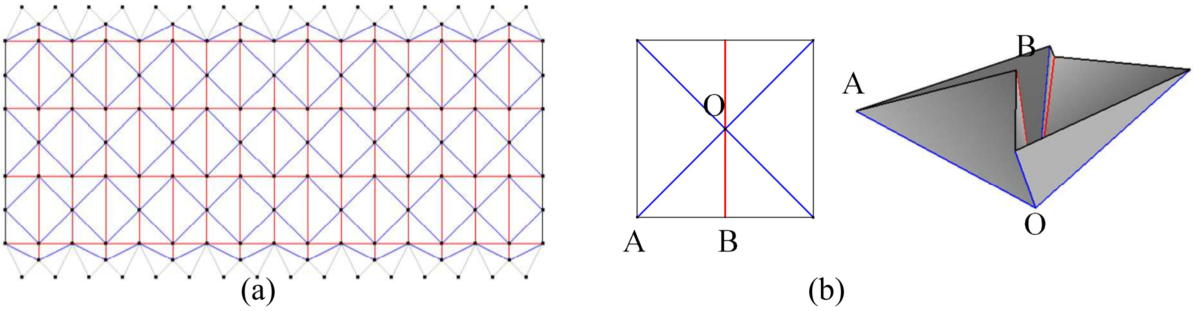

Figure 2 – Origami wheel pattern (a) redesigned by Lee *et al.* (2013), the waterbomb fold and a unitary cell (b).

2.1. Geometric Analysis

SMA actuators provide the change between limit configurations and the restitution is provided by a passive elastic spring fixed at acrylic plates at the ends of the wheel (Fig. 3). The SMA actuators have a thermomechanical coupling and are designed such that the ambient temperature is lower than the temperature at which the martensitic phase is stable ($T < T_M$). The acrylic plates are thin octagonal cobblestones with apothem b, used to pin the elastic spring. The basic component is assumed to be a square with size $2a$.

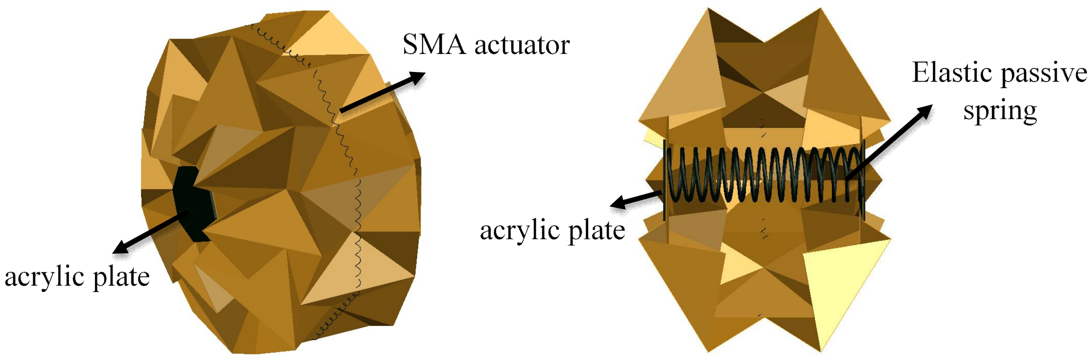

Figure 3 – Origami structure, with the actuators, the passive elastic spring and the acrylic plates.

For the next development, some hypotheses are of interest. First, assume that the structure is symmetrical. As a matter of fact, it is not strictly symmetric because of the end attachment of the origami structure. Once that this effect is so small that it can be neglected, the structure is assumed to be symmetric (Lee *et al.*, 2013). Thus, the force distribution is assumed to be homogeneous. Furthermore, once that this is a rigid origami, the folds occur only on the valley/ mountains. Therefore, all regions of the paper remain flat and the crease lines remain straight.

Looking at the unitary cell (Fig. 4), it is possible to obtain the first geometric relation. Assuming the coordinates $\mathrm{A}=(a\sin\theta, a, a\cos\theta)$, $\mathrm{B}=(0, a\sin\alpha, a\cos\alpha)$ and knowing that |AB|=a, it is possible to obtain the following equation:

$$\cos\theta\cos\alpha+\sin\alpha=1 \tag{1}$$

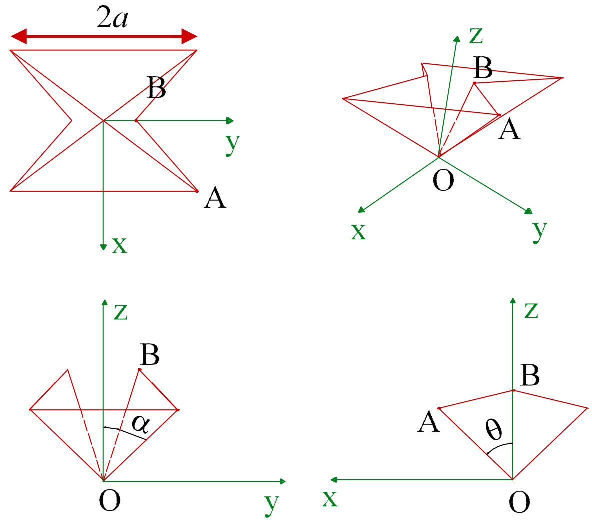

Figure 4 – Unitary cell of the origami wheel.

The origami structure is now divided into two views, as shows Fig. 5. The *X-Z* plan, circumferential view, includes the SMA actuators; the *Y-Z* plan, longitudinal view, includes the elastic passive spring. From *X-Z* plan it is possible to obtain the relations for the passive elastic spring half-length L_2 and the external origami radius R_2.

$$L_2=a\sin\alpha+2a\cos\beta-\frac{a}{2}\sin\beta \tag{2}$$

$$R_2=b+2a\sin\beta+\frac{a}{2}\cos\beta \tag{3}$$

From *X-Z* plan it is possible to obtain the relations for the actuator L_1, the internal radius of the origami wheel R_1 and the relation between the radii R_1 and R_2. Also, a relation for the radius R is obtained.

$$R_2=R_1+a\cos\alpha \tag{4}$$

$$L_1=2a\sin\theta \tag{5}$$

$$R_1=a\sin\left(\theta-\frac{\pi}{8}\right)\Big/\sin\frac{\pi}{8} \tag{6}$$

$$R=L_1\sqrt{\frac{2+\sqrt{2}}{2}} \tag{7}$$

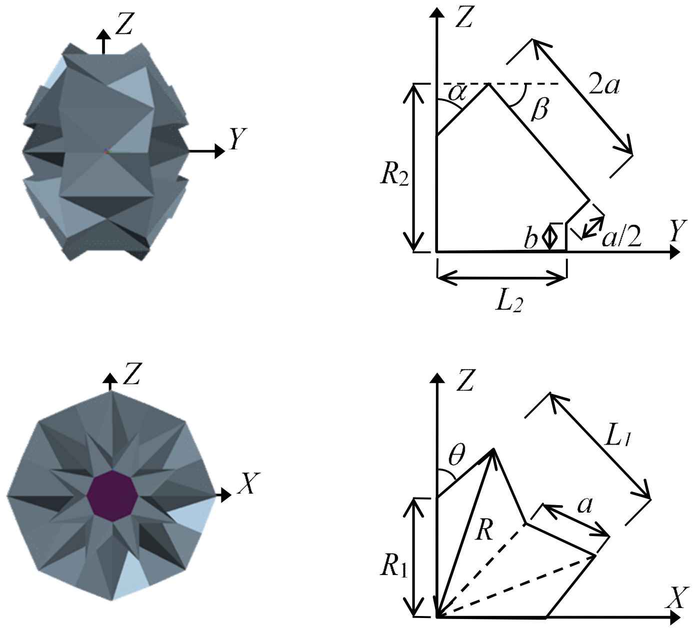

Figure 5 – Longitudinal (Y-Z plan) and circumferential (X-Z plan) views of the origami wheel.

By using equations (1) to (6), it is possible to find an explicit relation between L_2, R_1 or R_2 and L_1, as showed in Fig. 6 considering b = 0.04 m and a = 0.065 m. Figure 6-a shows the curve $L_2 = L_2\,(L_1)$ and Fig. 6-b shows the curves of the external radius R_2 and internal radius R_1 as a function of L_1. It is assumed, as initial condition, that both springs are free of tension with the SMA actuator in the martensitic phase and the origami wheel not totally opened. This means that SMA actuator has a residual strain that can be recovered by heating. It is important to be highlighted that, for the considered values of b and a, range of feasible values for constructive reasons is $L_1 \in [0.0555, 0.1225]$ m. In this regard, point P_0 represents the construction configuration (assumed as $L_1^0 = 0.109$ m for the adopted dimensions); point P_1 represents the minimum configuration, where the origami-wheel is completely closed (minimum radius); and point P_2 is the maximum configuration (origami-wheel completely opened). Figure 6 presents origami-wheel configuration characteristics.

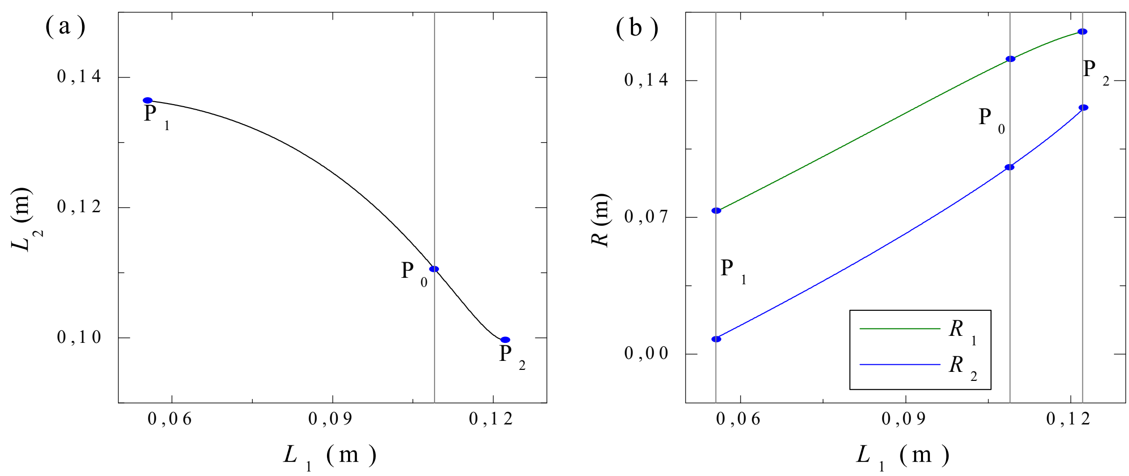

Figure 6 – Geometric relations of the origami-wheel. (a) Length of the passive spring in function of the length of the SMA spring. (b) Internal and external radii in function of the length of the SMA spring.

Table 1 – Configurations of the origami-wheel for *b* = 0.04m and *a* = 0.065m

	α (°)	β (°)	θ (°)	L_1 (m)	L_2 (m)	R_2 (m)	R_1 (m)
P_2	52.98	55.14	70.44	0.1225	0.0995	0.1652	0.1261
P_0	32.82	41.72	56.98	0.1090	0.1106	0.1508	0.0962
P_1	5.75	0.17	25.27	0.0555	0.1364	0.0729	0.0082
Maximum variation				0.0670	0.0369	0.0923	0.1179

3. STATIC ANALYSIS

Static analysis of the origami–wheel structure is now of concern considering actuator forces. A force E_2 applied in the longitudinal direction produces, by the effort transmission, a corresponding force in the radial direction E_1 (Fig. 7). Relation between these forces is provided by the following equation obtained by considering homogeneous distribution of efforts in all the structure:

$$E_1 = E_2 \frac{\cos\alpha + \sqrt{2}\cos\theta}{4\cos\beta} \tag{8}$$

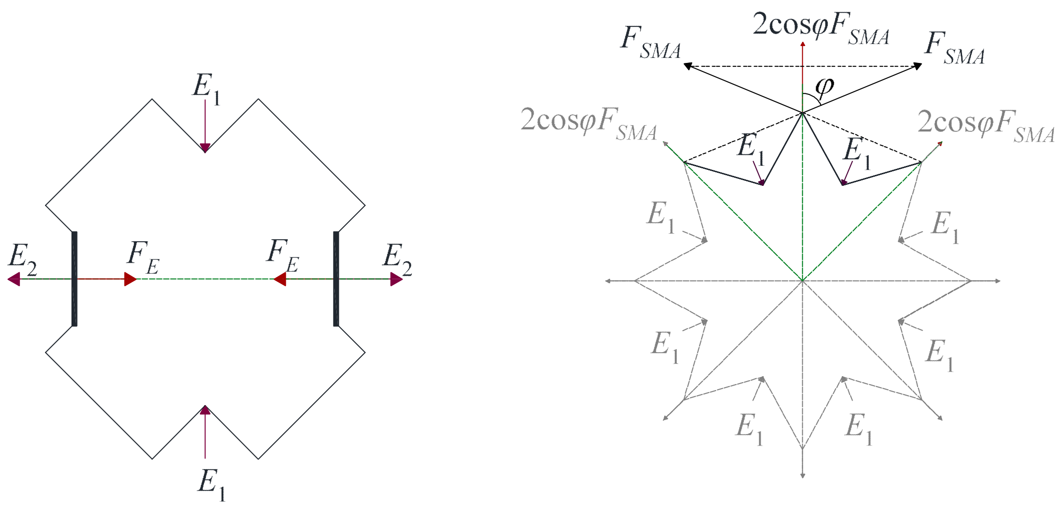

(a) (b)

Figure 7 – Free-body diagram in longitudinal (a) and circumferential (b) views.

The passive spring responds to the force E_2, producing a force F_E in the longitudinal direction. In the same way, SMA actuator produces a force F_{SMA} in the circumferential direction. By projecting F_{SMA} in the radial direction, since $\varphi = 45°$ due to the hypothesis that the structure is symmetrical and all unitary cells are squares, the equilibrium in the longitudinal and radial direction are given by:

$$\begin{cases} F_E = E_2 \\ \sqrt{2}F_{SMA} = E_1 \cos\dfrac{\pi}{8} \end{cases} \tag{9}$$

Combining these two equations by using equation (7), the sum of the forces is:

$$\sqrt{2}F_{SMA} - F_E \frac{\cos\alpha + \sqrt{2}\cos\theta}{4\cos\beta}\cos\frac{\pi}{8} = 0 \tag{10}$$

At this moment, it is important to describe the thermomechanical behavior of SMA by considering a constitutive model. This paper considers a polynomial constitutive model to establish a stress-strain-temperature relation (Falk, 1980, 1983; Paiva & Savi, 2006). Under this assumption, this one-dimensional model assumes a free energy that is represented by a sixth order polynomial as a function of strain and temperature. Based on that, three macroscopic phases are adopted: austenite, *A*, stable at high temperatures, and two variants of the martensite, *M*+ and *M*-, induced by tension and compression, respectively. The form of the polynomial is such that, at high temperatures, the free energy has only one minimum at vanishing strain; and at low temperatures, it has two minima at non-vanishing strains and a maximum at the vanishing strain.

Once that force-displacement-temperature relation of SMA springs is formally similar to stress-strain-temperature relations of SMA wires or bars (Aguiar *et al.*, 2010; Enemark *et al.*, 2016) and considering a helical spring with N coils with diameter D and wire diameter d, the SMA actuator restitution force can be written as follows:

$$F_{SMA} = \left(\frac{\pi d^3}{6D}\right)_{SMA}\left[c_1(T-T_M)\left(\frac{d}{\pi D^2 N}\right)_{SMA} u - c_2\left(\frac{d}{\pi D^2 N}\right)^3_{SMA} u^3 + c_3\left(\frac{d}{\pi D^2 N}\right)^5_{SMA} u^5\right] \tag{11}$$

where c_1, c_2 and c_3 are SMA material's constants, T_M represents the temperature bellow which the martensite phase is stable and T_A represents the temperature above which the austenite is stable. The restitution force of the passive elastic spring is described by a linear relation, where G is the shear modulus:

$$F_E = \left(\frac{G d^4}{6D^3 N}\right)_E u_E \tag{12}$$

The displacement of the passive elastic spring and the displacement of the SMA spring are given by $u_E = L_2 - L_2^0$ and $u = L_1 - L_1^0$, respectively, where the index "0" indicates the initial configuration (P_0). Thus, since L_2 can be written as function of L_1 through the Eq. (1) to (6), the displacement u_E can be written as a function of u.

Based on these relations, static equilibrium expressed in Eq. (10) is temperature dependent. By considering typical SMA parameters presented in Tab. 2, equilibrium curves are presented in Fig. 8 for different temperatures, assuming that the initial construction configuration temperature is at T_0 = 288 K. Note that at low temperatures ($T < T_A$) there are three positions where the sum of the forces vanishes and, at high temperatures ($T > T_A$), there is only one position where it occurs.

Table 2 – Material and system parameters

m (kg)	M (kg)	T_M (K)	T_A (K)	c_1 (MPa/K)	c_2 (MPa)	c_3 (MPa)
0.08	0.12	291.4	326.4	50	7.0×10^5	7.0×10^7
G_E (GPa)	d_E (m)	D_E (m)	N_E	d_{SMA} (m)	D_{SMA} (m)	N_{SMA}
80.0	3.0×10^{-3}	20.0×10^{-3}	30	2.0×10^{-3}	3.5×10^{-3}	10

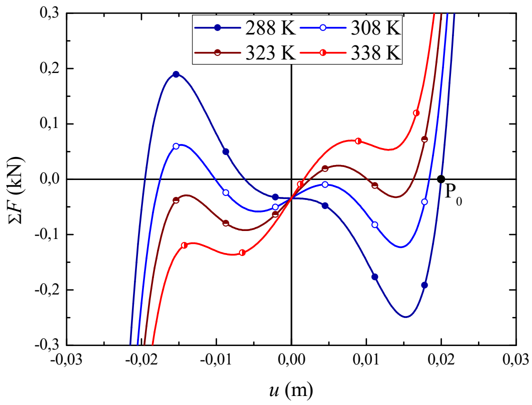

Figure 8 – Sum of the forces in a static equilibrium.

Figure 9 shows the structure behavior when the SMA actuator is subjected to a thermal load from T_0 =288 K to T = 373 K (Fig. 9-a). Figure 9-b presents the actuator displacements showing the longitudinal view of the origami. The displacement of the elastic spring due to the temperature change is much smaller when compared to the displacement of the SMA actuator. Figure 9-c shows that the length L_1 decreases from 0.109 m to 0.090 m (length variation of 0.019 m) while the length L_2 increases from 0.1106 m to 0.1119 m (length variation of 0.0013 m). The radius R_1 decreases from 0.096 m to 0.062 m and the radius R_2 decreases from 0.151 m to 0.124 m (Fig. 9-d).

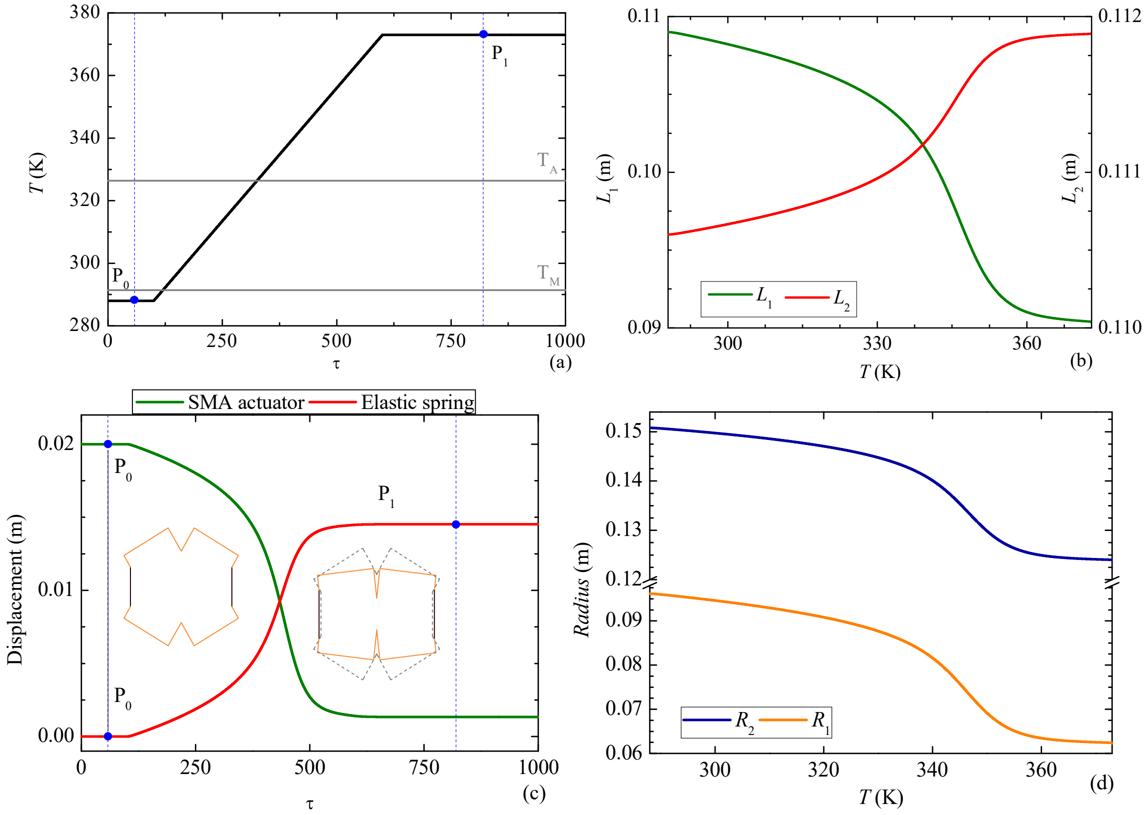

Figure 9 – Origami behavior due to temperature change. (a) Temperature load. (b) SMA and Elastic springs displacement. (c) SMA and Elastic spring length. (d) Internal and external radius variation.

4. DYNAMIC ANALYSIS

Origami system has a complex behavior with movements in several directions. Nevertheless, all these movements are geometrically coupled as discussed in the previous sections. Therefore, the dynamical behavior of the origami-wheel can be described by an equivalent one-degree of freedom oscillator (1-DOF) presented in this section.

The dynamical model considers that the structure mass can be discretized and has circumferential symmetry. Thus, assuming that the structure has a mass $8m$, the mass associated with each SMA actuator is m. Moreover, each acrylic plate has a mass M, which is associated with the half-length of the passive spring. Equations of motion are obtained adding inertia terms in the equilibrium equation as follows:

$$\begin{cases} M\ddot{u}_E + F_E = E_2 \\ m\ddot{r} + \sqrt{2}F_{SMA} = E_1 \cos\dfrac{\pi}{8} \end{cases} \tag{13}$$

where r represents the radial displacement of the mass associated with the SMA actuator (Eq. 7).

$$r = (L_1 - L_1^0)\sqrt{\frac{2+\sqrt{2}}{2}} \tag{14}$$

Equations (13) are coupled by Equation (8) and therefore, the following equation of motion is obtained:

$$M\ddot{u}_E - \frac{4\cos\beta}{\cos\frac{\pi}{8}(\cos\alpha + \sqrt{2}\cos\theta)}\left(m\ddot{r} + \sqrt{2}F_{SMA}\right) + F_E = 0 \tag{15}$$

Kinematics arguments are now assumed in order to rewrite the preceding equation of motion. First of all, the expression of u_E is obtained using Eq. (1) to (6). Note that $L_2 = L_2(L_1)$ presented in Fig. 6 can be rewritten in terms of displacements: $L_2 = L_2(L_1) = f(u)$. Then, assuming that $\ddot{f} = f_1(u)\ddot{u} + f_2(u)\dot{u}^2$ it is possible to write:

$$\ddot{u}_E = f_1\ddot{u} + f_2\dot{u}^2 \tag{16}$$

Equation (14) may be derived obtaining an expression for $\ddot{r}$:

$$\ddot{r} = \sqrt{\frac{2+\sqrt{2}}{2}}\ddot{u} \tag{17}$$

Using these expressions on Eq. (15), adding a linear viscous dissipation and an external force $F(t)$, it is possible to rewrite the equation of motion of the origami-wheel system.

Numerical simulations are carried out to investigate the nonlinear dynamics of the origami system. Numerical procedure employs the fourth order Runge-Kutta method and non-dimensional variables are adopted. Different operational conditions of the origami-wheel are treated considering thermal and mechanical external loads. Folding process, environmental variations and vehicle-ground interactions are some effects responsible for the proposed thermomechanical loads. Table 2 presents the parameters employed in all simulations together with a dissipation coefficient $\xi = 10^{-1}$.

Thermal loading process is represented by temperature variations responsible for SMA actuation and general fluctuations. Based on that, the following equations are considered,

$$T = \begin{cases} T_0, & \text{if } \tau < \tau_s \\ T^* + \mu\tau, & \text{if } \tau_s \le \tau \le \tau_f \\ T_f, & \text{if } \tau > \tau_f \end{cases} \tag{18}$$

where τ_s and τ_f corresponds to the start and finish of the thermal loading and $T^* = \left(T_0\tau_f - T_f\tau_s\right) \big/ \left(t_f - t_s\right)$. Parameter μ determines the temperature rate until a temperature T_f is reached.

Mechanical loading process considers that Fourier series may represent external loads. This kind of excitation may be caused by origami-ground interaction. For the sake of simplicity, only the first two terms are considered, being given by

$$F(\tau) = \sum_{i=1}^{n} \delta_i \cos\left(\omega_i\tau\right) \cong \delta_1 \cos\left(\omega_1\tau\right) + \delta_2 \cos\left(\omega_2\tau\right) \tag{19}$$

where $\delta_{1,2}$ are the dimensionless amplitude and $\omega_{1,2}$ are the dimensionless frequency of the mechanical load.

The dynamical analysis of the dissipative origami-system starts with configuration change induced by thermal loading. Therefore, consider a temperature change from T = 288 K to T = 343 K, without external mechanical load. Figure 10 shows the thermal load and the corresponded displacements. Note that inertia causes oscillations before the system reaches the final configuration.

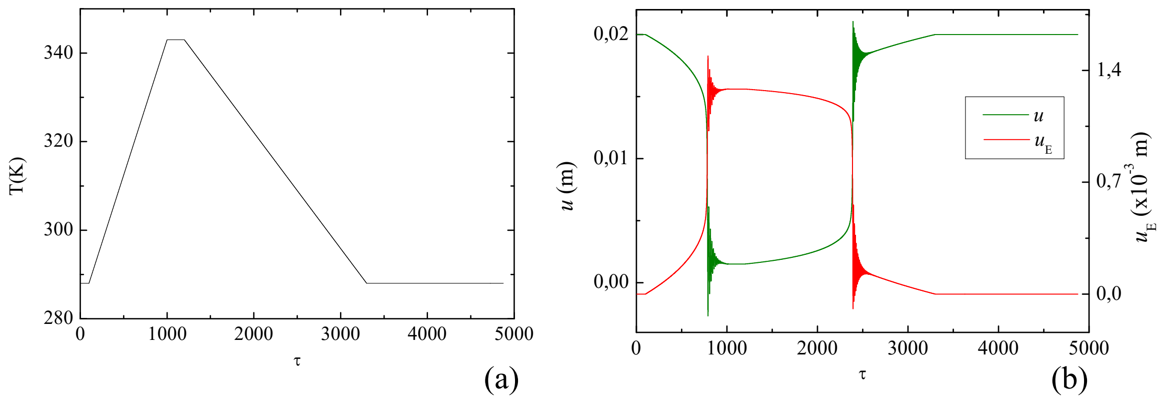

Figure 10 – Origami with temperature changes. (a) Thermal loading. (b) Origami response.

A mechanical loading process is now of concern assuming a constant temperature T = 343 K and loading represented by δ_1 = 10-3, ω_1 = 0.8, $\delta_2 = 7\times10^{-4}$ and ω_2 = 3. Figure 11-a presents the origami dissipative response (ξ=0.1). Under these conditions, a period-4 response is observed. In a non-dissipative system (ξ=0), a quasi-periodic response is observed as shown in Fig. 11-b in the form of phase space together with Poincaré section. By decreasing the temperature for the non-dissipative system (T = 288 K), beat phenomena is observed (Fig. 12).

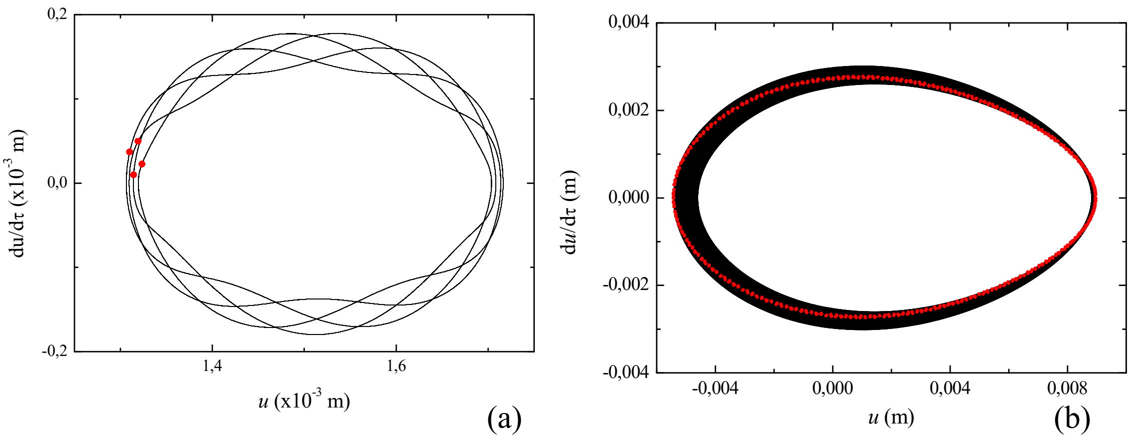

Figure 11 – Phase space and Poincaré sections for T = 343 K. (a) ξ=0.1. (b) ξ=0.

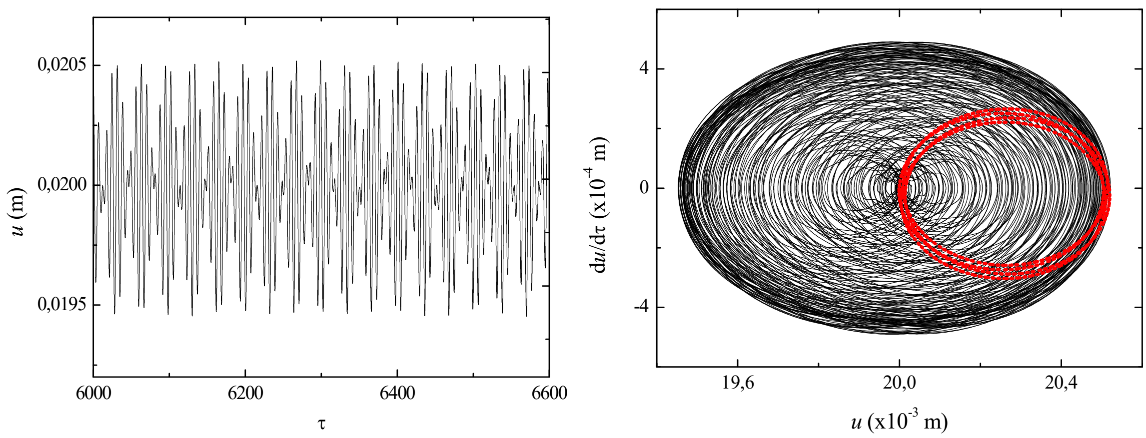

Figure 12 – Origami response due to mechanical loads with T = 288 K and ξ = 0.

Complex responses are possible in origami systems. A chaotic response of the origami-wheel is presented by considering δ_1=0.024. Other forcing parameters are ω_1=0.8, δ_2=7×10-4 and ω_2=3. Besides that, a constant temperature T = 288K and a dissipation of ξ=0.1 are adopted. Phase space associated with a typical strange attractor is observed in Figure 13. Lyapunov exponents estimated with the algorithm due to Wolf *et al.* (1985) assure this conclusion presenting a positive maximum value 0.24, with a fractal dimension 1.74, estimated by the Kaplan-Yorke conjecture

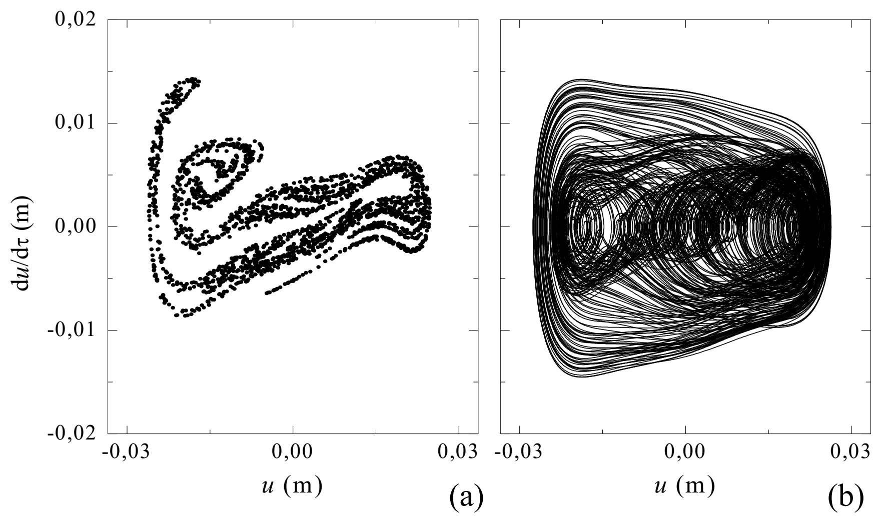

Figure 13 – Poincaré section (a) and phase space (b) for T = 288K, δ_1 = 0.024, δ_2 = 7×10^{-4}, ω_1 = 0.8, ω_2 = 3 and ξ=0.1.

5. CONCLUSIONS

This paper deals with the dynamical analysis of origami-wheel system actuated by shape memory alloy actuators. Basically, a one-degree of freedom system is proposed to explore the system behavior. A polynomial constitutive model is employed to describe the thermomechanical behavior of the SMAs. Construction and operational conditions are carried out considering different thermomechanical loading processes. Harmonic mechanical excitations represent different origami-ground interactions. Numerical simulations are carried out showing rich dynamical behavior, with periodic, quasi-periodic and chaotic responses.

6. ACKNOWLEDGMENTS

The authors would like to acknowledge the support of the Brazilian Research Agencies CNPq, CAPES and FAPERJ and through the INCT-EIE (National Institute of Science and Technology - Smart Structures in Engineering) the CNPq and FAPEMIG. The Air Force Office of Scientific Research (AFOSR) is also acknowledged.

7. REFERENCES

Aguiar, R. A. A., Savi, M. A. & Pacheco, P. M. C. L. (2010), “Experimental and Numerical Investigations of Shape Memory Alloy Helical Springs”, Smart Mater. Struct., v. 19, pp. 025008.

Enemark, S., Santos, I. & Savi, M. A. (2016), “Modelling, characterisation and uncertainties of stabilised pseudoelastic shape memory alloy helical springs”, Journal of Intelligent Material Systems and Structures, doi:10.1177/1045389X16635845.

Falk, F. (1980), “Model free-energy, mechanics and thermodynamics of shape memory alloys”, ACTA Metallurgica, v. 28, n. 12, pp. 1773–1780.

Falk, F. (1983), “One-dimensional model of shape memory alloys”, Archives of Mechanics, v. 35, n. 1, pp. 63–84.

Fei, L. J. & Sujan, D. (2013), “Origami theory and its applications: A Literature review”, International Journal of Social Behavioral, Educational, Economic and Management Engineering, v. 7, n. 1, pp. 113–117.

Felton, S., Lee, D. Y., Cho, K. J. & Wood, R. J. (2014), “A Passive, Origami-Inspired, Continuously Variable Transmission”, in IEEE International Conference on Robotics and Automation, pp. 2913–2918.

Lee, D. Y., Jung, G. P., Sin, M. K., Ahn, S.H. & Cho, K. J. (2013), "Deformable wheel robot based on origami structure", IEEE Int. Conf. on Robotics and Automation (ICRA), pp. 5592 -5597.

Lee, D. Y., Kim, J. S., Kim, S. R., Koh, J. S.& Cho, K. J. (2013), “The deformable wheel robot using magic-ball origami structure”, Proc. of the ASME 2013 Int. Design Engineering Technical Conf. & Computers and Information in Engineering Conf. (IDETC/CIE).

Nishiyama Y. (2012), “Miura folding: applying origami to space exploration”, International Journal of Pure and Applied Mathematics, v. 79, pp. 269-179.

J. Mitani. Oripa; origami pattern editor. http://mitani.cs.tsukuba.ac.jp/pukiwiki-oripa/, 2005.

Paiva, A. & Savi, M. A. (2006), “An overview of constitutive models for shape memory alloys, Mathematical Problems in Engineering”, 1-30, article ID56876.

Peraza-Hernandez, E. A., Hartl, D. J., Malak Jr, R. J.& Lagoudas, D. C. (2014), “Origami-inspired active structures: a synthesis and review”, Smart Materials and Structures, v. 23, pp. 094001.

Salerno, M., Zhang, K., Menciassi, A. & Dai, J. S. (2014), “A Novel 4-DOFs Origami Enabled, SMA Actuated, Robotic End-effector for Minimally Invasive Surgery”, in IEEE International Conference on Robotics and Automation (ICRA), pp. 2844-2849.

Sorguç, A., Hagiwara, I. & Selçuk, S. (2009), “Origamics in architecture: a medium of inquiry for design in architecture”, METU Journal of the faculty of architecture, 26:2, pp. 235-247.

Wolf, A., Swift, J. B., Swinney, H. L. & Vastano, J. A. (1985), “Determining Lyapunov Exponents from a Times Series”, Physica D, v. 16, pp. 285–317.

8. RESPONSIBILITY NOTICE

The authors are the only responsible for the content of this work.